Catalysis Science & Technology

ROYAL SOCIETY OF CHEMISTRY

PAPER

View Article Online
View Journal | View Issue

Cite this: *Catal. Sci. Technol.*, 2022, 12, 6676

Observation of surface species in plasma-catalytic dry reforming of methane in a novel atmospheric pressure dielectric barrier discharge *in situ* IR cell†

Joran Van Turnhout, [ab] Domenico Aceto,[bc] Arnaud Travert,[b] Philippe Bazin,[b] Frédéric Thibault-Starzyk,[b] Annemie Bogaerts [a] and Federico Azzolina-Jury*[b]

Received 16th February 2022,
Accepted 26th September 2022

DOI: 10.1039/d2cy00311b

rsc.li/catalysis

We developed a novel *in situ* (*i.e.* inside plasma and during operation) IR dielectric barrier discharge cell allowing investigation of plasma catalysis in transmission mode, atmospheric pressure, flow conditions (WHSV ~0–50 000 mL g^{-1} h^{-1}), at relevant discharge voltages (~0–50 kV) and frequencies (~0–5 kHz). We applied it to study the IR-active surface species formed on a SiO_2 support and on a 3 wt% Ru/SiO_2 catalyst, which can help to reveal the important surface reaction mechanisms during the plasma-catalytic dry reforming of methane (DRM). Moreover, we present a technique for the challenging task of estimating the temperature of a catalyst sample in a plasma-catalytic system *in situ* and during plasma operation. We found that during the reaction, water is immediately formed at the SiO_2 surface, and physisorbed formic acid is formed with a delay. As Ru/SiO_2 is subject to greater plasma-induced heating than SiO_2 (with a surface temperature increase in the range of 70–120 °C, with peaks up to 150 °C), we observe lower amounts of physisorbed water on Ru/SiO_2, and less physisorbed formic acid formation. Importantly, the formation of surface species on the catalyst sample in our plasma-catalytic setup, as well as the observed conversions and selectivities in plasma conditions, can not be explained by plasma-induced heating of the catalyst surface, but must be attributed to other plasma effects, such as the adsorption of plasma-generated radicals and molecules, or the occurrence of Eley–Rideal reactions.

1. Introduction

In the fight against climate change, the dry reforming of methane (DRM) has gained significant interest for the conversion of greenhouse gases (GHGs) into value-added chemicals. Indeed, this reaction involves the conversion of CO_2 and CH_4, the two main greenhouse gases, into syngas. The latter is a valuable feedstock for gas-to-liquid (GTL) technology *via* the Fischer–Tropsch synthesis, and can also be used for methanol synthesis.[1] However, despite its rich history, DRM remains a significant challenge in chemical engineering. Indeed, high operating temperatures (400–1000 °C) and significant coking of the used catalysts (typically containing Ni, Co or precious metals) form grave limitations for the thermo-catalytic DRM, so that it is not yet widely used on an industrial scale today.

A possible alternative is the combination of a catalyst with non-thermal plasma (NTP). In such a plasma-catalytic system, inelastic collisions of high-energy electrons with reactant molecules lead to the production of reactive and excited species, thus enabling the activation of CO_2 and CH_4 near room temperature.[2–4] Concurrently, reactive species formed in the plasma can interact with the catalyst and thus change its properties, and *vice versa*, the presence of a catalyst in the plasma influences the plasma properties;[6] this can give rise to synergetic effects, which can yield an enhanced conversion,[7] improved selectivity towards targeted reaction products,[3–5] improvement of the energy efficiency,[6,8] and may enhance the catalyst stability by reducing coke formation and sintering.[9,10]

Among the many types of NTP that are being investigated, a dielectric barrier discharge (DBD) is the most suitable for plasma catalysis, because its simple design allows for easy implementation of catalyst material into the discharge zone, it operates near room temperature, is easily switched on and off, is simple to operate and scale up, and operates under atmospheric pressure.[11] Currently, for DRM, packed bed DBDs can provide conversions of up to 80% with an energy cost in the range of 15–100 eV per molecule,[12] which is much higher than the set benchmark of 4.27 eV per molecule (*i.e.*

[a] *Research group PLASMANT, Department of Chemistry, University of Antwerp, 2610 Wilrijk-Antwerp, Belgium*
[b] *Laboratoire Catalyse et Spectrochimie (LCS), ENSICAEN, UNICAEN, CNRS, Normandie Univ, 14000 Caen, France. E-mail: federico.azzolina-jury@ensicaen.fr*
[c] *CQE-DEQ, Instituto Superior Técnico, Universidade de Lisboa, 1049-001 Lisboa, Portugal*

† Electronic supplementary information (ESI) available. See DOI: https://doi.org/10.1039/d2cy00311b

energy efficiency of 60%) as proposed by Snoeckx and Bogaerts,[12] in order for plasma-catalytic syngas formation to be a competitive alternative to thermal catalysis. Clearly, significant improvement is required in order for plasma-catalytic syngas production to be a viable approach. For this, a better understanding of the plasma-catalytic synergy is paramount.

Plasma-catalytic synergy can be partly attributed to plasma-induced changes in catalyst surface reaction pathways. For example, highly reactive plasma species (like radicals) may have a larger sticking probability on the catalyst surface than their molecular counterparts, paving the way for new reactive pathways on the surface.[6] Additionally, reactive plasma species are more likely to react with adsorbed species *via* Eley–Rideal mechanisms,[9] whereas in thermal catalysis surface reactions overwhelmingly occur *via* the Langmuir–Hinshelwood mechanism.[13,14] Moreover, high-energy electrons in the plasma may influence the reactions on the catalyst surface.[9,15] Finally, vibrationally excited species may play an important role in the plasma-catalytic synergy.[16–18] All of the above implies that for a certain reaction, the optimal plasma catalyst may differ significantly from the optimal thermal catalyst. Indeed, this was already shown computationally for other plasma-catalytic systems.[16,18]

Clearly, a thorough understanding of the effects of NTP on catalyst surface chemistry is paramount for the rational design of a plasma-catalytic system. While microkinetic models[16–19] and DFT studies[8] can provide useful insights in the possible effect of plasma on the catalytic surface chemistry, their accuracy is inherently limited by approximations and therefore, experimental validation to those models is imperative. For this, *in situ* (*i.e.* inside the plasma, during operation) IR spectroscopy analysis of catalyst surface species is particularly interesting.

In previous work, *in situ* observation of species at the catalyst surface in plasma catalysis has mostly been performed by diffuse reflectance infrared Fourier transform spectroscopy (DRIFTS),[10,20–23] a sampling technique widely used in thermal catalysis. Alternatively, transmission IR can be applied. Advantages of the latter include (i) the possibility for relatively straightforward quantitative studies, as transmission FTIR obeys the Beer–Lambert law, in contrast to DRIFTS, which follows the Kubelka–Munk theory, (ii) lower temperature dependence, (iii) the elimination of grain size dependence and (iv) a smaller temperature gradient in the catalyst material.[24,26] While previously developed transmission cells allowed for the analysis of surface species at low pressures under flow conditions[25,40,41] or in a closed system at atmospheric pressure,[27] to date, no transmission IR cell has allowed the study of DBD plasma catalysis under continuous flow at atmospheric pressure.

To the best of our knowledge, to this day, only one publication[22] reported an *in situ* IR study of plasma-catalytic DRM using DRIFTS, and the influence of NTP on catalyst surface species in DRM is largely unexplored. Therefore, in the present work, we describe a novel *in situ* DBD IR cell that allows for investigation of plasma catalysis in a DBD in transmission mode, atmospheric pressure, flow conditions (WHSV ~0–50 000 mL g^{-1} h^{-1}), relevant discharge voltages (~0–50 kV) and frequencies (~0–5 kHz) and temperatures up to 450 °C. We applied it for the first time to study the surface species formed during plasma-catalytic DRM over SiO_2 and 3 wt% Ru/SiO_2. Ru has shown promising results for thermo-catalytic DRM,[28] and SiO_2 was chosen as an inert support in an attempt to minimize the contribution of the support to the catalytic activity of the metal-loaded material. Moreover, we also tested both SiO_2 and Ru/SiO_2 in a packed bed DBD reactor, and measured the CO_2 and CH_4 conversion, as well as the product yields and selectivities, in order to link the observations of our *in situ* experiments to the catalytic activity.

Finally, it is crucial to know the catalyst surface temperature during plasma catalysis, to better understand the underlying mechanism, *i.e.*, whether the formation of surface species is due to plasma-induced heating of the catalyst surface or due to other plasma effects, such as plasma-generated radicals. However, *in situ* measurement of the catalyst surface temperature inside a DBD plasma is particularly challenging. To our knowledge, it has only been reported twice in literature, and for other reactions than DRM.[23,29] In this work, we provide a novel technique to estimate the temperature of the catalyst wafer under DBD plasma using FTIR spectroscopy in the *in situ* DBD IR cell.

2. Experimental

2.1. Catalyst preparation and characterization

Ru loading of the SiO_2 support (Solvay) was carried out by wet impregnation (3 wt% Ru) using $RuCl_3{\cdot}xH_2O$ (Sigma Aldrich, 99.98%) as precursor salt dissolved in H_2O. Note that the provider did not specify the hydrate of the salt, and therefore we estimated the metal loading using EDS-SEM (see section 3.1). The water was evaporated under continuous stirring using a rotary evaporator at 70 °C under vacuum (0.3 Torr) until complete dryness. Afterwards, the catalyst powder was calcined at 450 °C for 4 h and subsequently reduced at its reduction temperature as determined by TPR (see section 3.1) for 4 h in a gas mixture of 20 vol% H_2 and 80 vol% Ar with a total gas flow rate of 16 mL min^{-1} (STP). Finally, for the transmission IR measurements, the catalyst powder was pressed (1 ton, 10 s) into wafers (2 cm^2, ~20 mg). For the packed bed experiments, the catalyst powder was shaped into irregular extrudates (>1 mm in every dimension). For this, 50 mg of the catalyst material was pressed (2 tons, ~5 seconds) in a pellet with height > 1 mm. The pellet was crushed and the pieces were sieved to select only those having each dimension > 1 mm, to guarantee gaps in the catalyst bed that are larger than the Debye length of the plasma (typically 0.5–1 μm for DBD). The shaping of SiO_2 for experiments on the support alone was done similarly to the shaping of the metal-loaded SiO_2.

H_2 temperature programmed reduction (H_2-TPR) was applied to the catalyst pre thermal reduction in order to determine the reduction temperature of the deposited metal oxide particles on the support. For this, 0.05 g of a catalyst sample was heated to 1000 °C in a 5 vol% H_2 and 95 vol% Ar gas flow (total flow rate of 40 mL min^{-1} (STP)) at a heating rate of 10 °C min^{-1} using a Micromeritics Autochem II chemisorption analyser equipped with a thermal conductivity detector and subsequently cooled down to room temperature.

X-ray diffraction patterns of the Ru/SiO_2 catalyst were recorded post-reduction with a PANalytical X'pert PRO diffractometer with CuKα radiation (λ = 0.15418 nm, 40 mA, 45 kV). The sample was scanned from 5 to 80° at a step size of 0.0083556° and scanning rate of 0.026526° min^{-1}.

The specific surface area (SA) and pore volume of the catalyst and SiO_2 support were determined by N_2-physisorption measurements at −196 °C using a Micromeritics ASAP 2020 Plus adsorption analyser. Before N_2-adsorption, the sample (0.2 g) was degassed at 200 °C overnight. The specific SA of the sample was calculated using the Brunauer, Emmett and Teller (BET) method. The total pore volume was measured at P/P^0 = 0.99.

Energy-dispersive X-ray spectroscopy (EDS) coupled to scanning electron microscopy (SEM) was used for the elemental analysis of Ru/SiO_2 catalyst using an EDAX XM2-30T apparatus. Two separate regions of the catalyst were analysed.

2.2. *In situ* IR

2.2.1. Experimental setup. A schematic representation of the novel *in situ* DBD IR cell used for transmission IR measurements is given in Fig. 1. A more detailed scheme and photographs of the cell can be found in the ESI† (section S1; Fig. S1–S3).

The H_2, CH_4, CO_2 and Ar gas inlet is controlled by four separate Brooks Delta Smart II mass flow controllers. The gas inflow is mixed and introduced in the glass DBD cell. The gas outlet is placed higher up in the cell and is connected to a Pfeiffer Vacuum Prisma Pro quadrupole mass spectrometer to monitor the outlet gas composition. Additionally, the cell is connected to a rotary pump (~0.3 Torr, Edwards nXDS6iC) and turbopump (10^{-7} Torr, Pfeiffer vacuum HiCube 80) to allow for easy purging of the cell.

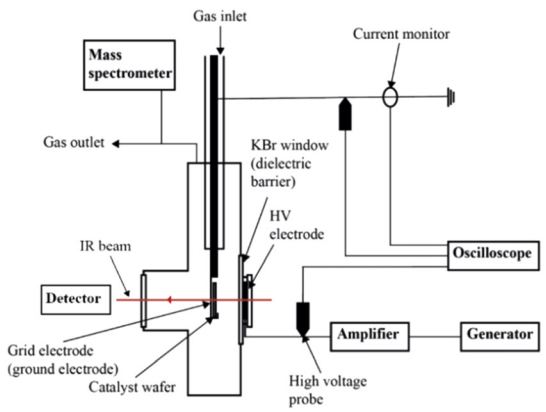

Fig. 1 Schematic representation of the novel *in situ* DBD IR cell.

The DBD IR cell is positioned inside the sample compartment of a Bruker Vertex 80 V spectrometer with a liquid nitrogen cooled mercury–cadmium–telluride (MCT) detector. The glass cell is sealed with two KBr windows for the IR beam to pass through, ensuring an IR transmission window in the 4000–400 cm^{-1} range. The catalyst is introduced as a wafer in the sample holder, which is attached to a grid electrode. Parallel to this electrode, a similar grid electrode is placed behind one of the aforementioned KBr windows; the latter functions as a dielectric barrier. This electrode is electrically isolated with a third KBr window. The gap between both electrodes is ~5 mm.

The inner grid electrode is grounded, whereas the outer grid electrode is connected to a signal generator (Générateur de fonctions arbitraires 50 MHz, Française d'Intrumentation) which is amplified (Trek 20/20C). A voltage probe (Testec HVP-2739-1000:1) is placed on the connection between the outer high voltage (HV) electrode and the amplifier. Additionally, a voltage probe is positioned on the connection between the inner ground electrode and the ground, and a current monitor (Hioki CT6710) is placed on this same connection. The voltage and current probes are connected to a Tektronix MDO3024 oscilloscope. The latter illustrates a significant advantage of our cell, being that our setup allows for continuous measurement of plasma parameters during an experiment.

2.2.2. *In situ* observation of surface species. After being introduced into the cell, the Ru/SiO_2 wafer was activated at 350 °C for 1.5 h under secondary vacuum (10^{-7} Torr) after which the catalyst was kept at the same pressure for 16 h. The cell was subsequently filled with Ar to a pressure of 1 atm and an Ar plasma was ignited at a voltage of ~16 kV, a frequency of 3 kHz and an Ar gas flow rate of 20 mL min^{-1} (STP). Next, the gas flow was changed to 20 vol% H_2 and 80 vol% Ar (20 mL min^{-1} total, STP) and the voltage was increased to ~28 kV to sustain the plasma. In this way, the catalyst was reduced *in situ* for 20 min. Afterwards, the plasma was extinguished and the cell was purged under vacuum (0.3 Torr) in order to remove the water formed during the reduction step.

After the purging that followed the *in situ* reduction, the cell was filled with a gas flow of 20 mL min^{-1} (STP) consisting of 35 vol% CH_4, 35 vol% CO_2 and 30 vol% Ar to a pressure of 1 atm. Then, plasma was again ignited at a voltage of ~30 kV and a frequency of 3 kHz. The Ar in the system was necessary to sustain the discharge. After reaching a stable conversion (measured with the mass spectrometer), the plasma was extinguished and the outlet gas flow was again stabilized. Subsequently, the system was put under vacuum (0.3 Torr) to purge the cell and to monitor the adsorbed species on the catalyst surface. Then, we heated the catalyst pellet *in situ* to set temperatures to monitor the desorption behaviour of

strongly adsorbed species as a function of temperature. Note that the catalyst surface (and gas around the surface) was continuously monitored during both the *in situ* reduction and the DRM reaction using transmission FTIR (resolution of 4 cm^{-1}, 64 scans per spectrum and 1 spectrum recorded per 9 s) as described in section 2.2.1 above.

In addition to the tests with the Ru/SiO_2-loaded sample holder, a test was performed with the SiO_2 support and in the empty (*i.e.* no wafer in the sample holder) cell. For the former, no *in situ* reduction was required, while for the latter neither activation, nor *in situ* reduction was required. The rest of the protocol remained identical.

Note that while, in principle, the presence of a mass spectrometer at the gas outlet should allow for *operando* operation (*i.e.* activity measurements in parallel to surface characterization), the operation under plasma conditions requires spatial separation of the electrodes from any metallic parts of the spectrometer, leading to large dead volumes in the current cell. Measured conversions are therefore very low (see Table S2†), so that we proceed with activity testing in a packed bed DBD reactor (see section 2.3). However, it is noteworthy that, while the observed conversions in our *in situ* cell are much lower, the observed selectivity towards CO and H_2 on both SiO_2 and Ru/SiO_2 show similar values to the ones obtained in the packed bed reactor below (see Table S2†).

2.2.3. *In situ* temperature measurements. $BaSO_4$ was used as an internal standard for temperature measurements. This salt presents absorption bands of low intensity near 2000 cm^{-1}, which can be assigned to overtone and combination bands of low wavenumber stretching and bending S–O vibrations.[35,36] These bands were observed to experience a downward frequency shift (bathochromic shift) with the increase of the sample temperature. A band located at 1965.9 cm^{-1} at room temperature and not overlapping with vicinal bands was used to establish a temperature scale based on the position of its maximum $\tilde{\nu}_{max}$ measured in a temperature-calibrated IR cell. The calibration curve yielded the following equation (R^2 = 0.997, SD = 5 °C):

$$t/°C = -35.30985 \times \tilde{\nu}_{max}/cm^{-1} + 69\,442.7 \quad (1)$$

Experiments were performed with either a wafer of 40 mg of pure $BaSO_4$ in a H_2/Ar plasma or wafer of a mixture of 10 mg of Ru/SiO_2 powder with 30 mg of $BaSO_4$ (Alfa Aesar, 97%). The determination of the position of band maxima for calibration and measures was carried out by quadric interpolation with SpectroChempy.[38,39]

2.2.4. Thermal *in situ operando* IR "sandwich" cell. To distinguish the effect of plasma-induced heating from other plasma effects, the Ru/SiO_2 wafer was also tested in a thermal *in situ operando* IR "sandwich" cell at 100 and 150 °C (*i.e.* around the observed temperature range of the catalyst wafer in the plasma, as described in section 3.2.3). More information on the setup and experimental procedure is available in the ESI† (section S6).

2.3. Packed bed DBD

2.3.1. Experimental setup. The packed bed reactor consists of a cylindrical inner electrode (stainless steel, $Ø$ = 5 mm) positioned at the centre of a glass cylinder ($Ø_{inner}$ = 10 mm) which is surrounded by the outer electrode (Cu coil, L = 100 mm). Thus, a discharge gap of 2.5 mm is obtained. Catalyst material is positioned in the discharge zone (*i.e.* within the gap between the electrodes) and is held in place with silicon wool, which is positioned right underneath the discharge zone. A scheme of the DBD packed bed reactor is given in the ESI† (Fig. S4).

The outer coil electrode is grounded, whereas the inner rod electrode is connected to a signal generator (Générateur de fonctions arbitraires 50 MHz, Française d'Intrumentation) which is amplified (Trek 20/20C). The voltage and current during the experiment are monitored similarly to the *in situ* setup as described above.

Likewise, the H_2, CH_4, CO_2 and Ar gas inlet control, as well as the analysis of the outlet gas, is executed similarly to the *in situ* setup described above.

In one experiment for both SiO_2 and Ru/SiO_2, IR spectroscopy is used to detect the presence of higher hydrocarbons or oxygenates such as methanol in the outlet gas. Thus another line is added between the mass spectrometer and the gas exhaust, leading to a glass cell positioned inside the sample compartment of a Bruker Vertex 80 V spectrometer with a liquid nitrogen cooled mercury–cadmium–telluride (MCT) detector. The glass cell is sealed with two KBr windows for the IR beam to pass through, ensuring an IR transmission window in the 4000–400 cm^{-1} range.

2.3.2. Experimental procedure. First, the discharge gap was packed with reduced 3 wt% Ru/SiO_2 extrudates (1.5 g). Then, the setup was purged under vacuum (~0.3 Torr), and the DBD packed bed reactor was subsequently filled with Ar to 1 atm. The catalyst was reduced *in situ* at 350 °C for 1.5 h under a gas flow of 20 vol% H_2 in Ar (total of 45 mL min^{-1}, STP) after which the system was kept under vacuum (~0.3 Torr) for 2 h. The catalyst was again treated *in situ* using H_2/Ar plasma as described for the *in situ* cell, with the only difference being the applied voltage (20 kV) and duration (10 min) to limit the strain on our reactor.

Likewise, the continuation of the experiment was similar to the procedure described for the *in situ* cell described above. However, for the packed bed reactor, we used a total gas flow rate of 22 mL min^{-1} (STP) and applied a voltage of 25 kV, as further increasing the voltage led to arc discharges, making safe operation impossible. Moreover, to allow for easier discharging, plasma was ignited in pure Ar first, after which the reactant gases were introduced.

The outlet gas was continuously monitored using mass spectrometry. More specifically, the following mass-to-charge ratios (m/z) were monitored using PV MassSpec software: 2 (H_2), 15 (CH_3, as a proxy for CH_4, to avoid interference with O), 28 (CO), 40 (Ar) and 44 (CO_2). The contribution of CO_2 to

the m/z = 28 signal was accounted for during quantitative data processing to avoid an underestimation of CO production. The experiments were executed three times. In one experiment, the outlet gas was also monitored using FTIR to detect the presence of higher hydrocarbons or oxygenates such as methanol. Another experiment was run (again three times) with SiO_2 support alone following the same procedure, but without *in situ* reduction.

The formulas used for the calculation of CO_2 and CH_4 conversion, and for the product yields and selectivities, are given in section S2 of the ESI.† The calibration curves for these calculations are given in section S3 of the ESI† (Fig. S5–S10).

3. Results and discussion

3.1. Catalyst characterization

Detailed catalyst characterization is presented in section S4 of the ESI.† The H_2-TPR profile of the Ru-loaded catalyst shows a peak at 166 °C corresponding to the reduction of RuO_2 to metallic Ru (see Fig. S11†). A smaller peak was found at 417 °C, possibly indicating the reduction of Ru clusters on the SiO_2 support.

The X-ray diffractogram of the amorphous SiO_2 support shows a broad peak at 2θ = 23°. The 3 wt% Ru/SiO_2 sample shows a minor peak at 2θ = 44° corresponding to Ru(101) (see Fig. S12†). A complete reduction of RuO_2 to metallic Ru is indicated by the absence of peaks at 2θ = 28°, 35° and 54°, corresponding to RuO_2(110), RuO_2(101) and RuO_2(211), respectively.

The SiO_2 support and 3 wt% Ru/SiO_2 catalyst exhibit a BET surface area of 151 and 148 $m^2\ g^{-1}$, respectively. The weight loss upon degassing, which is a measure for the water holding capacity of the samples, is 9 and 5 wt% for the SiO_2 support and the 3 wt% Ru/SiO_2 sample, respectively. The isotherms (see Fig. S13 and S14†), being of type IVa in the IUPAC classification of physisorption isotherms, suggest a mesoporous adsorbent with pores wider than 4 nm. The hysteresis loop of the samples can be classified as type H2b, suggesting the presence of small pore necks with a large size distribution.

The presence of Ru was confirmed using EDS-SEM. Fig. 2 shows the Ru distribution in two analysed regions of the Ru/SiO_2 catalyst. Clearly, the Ru distribution over the SiO_2 support is mostly homogeneous, although some Ru clusters of ~1 μm have been observed on the SiO_2 surface. Additionally, trace amounts of Al and Na appear to be present, possibly due to impurities in the SiO_2 support (see Table S1, Fig. S15 and S16†). Finally, we estimate a Ru loading of ~5 wt% (see Fig. S17†).

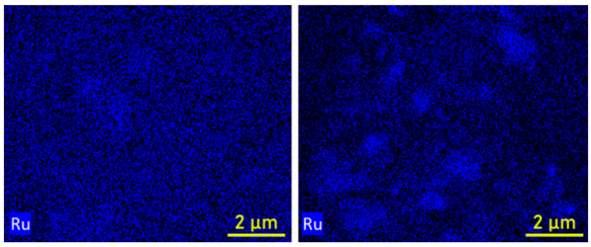

Fig. 2 EDS elemental mapping of two spots on the Ru/SiO_2 catalyst, showing a homogeneous Ru loading on the SiO_2 support with additional presence of larger (~1 μm) Ru clusters.

3.2. *In situ* IR

3.2.1. SiO_2 support. In order to disentangle the effects of the individual reactants of DRM (*i.e.* CO_2 and CH_4), we performed experiments with CO_2/Ar and CH_4/Ar plasma in addition to experiments with a mixture of the reactants. The results of these experiments are presented in section S5 of the ESI† (Fig. S18–S24). The FTIR difference spectra (3800–2400 cm^{-1}), recorded during DRM in plasma on the SiO_2 support are shown in Fig. 3.

A characteristic IR band of gas phase CH_4 can be observed at 3015 cm^{-1} and is ascribed to the ν_3 mode of CH_4. Moreover, the presence of gas phase CO_2 is evidenced by the combination bands at 3727 and 3703 cm^{-1} ($\nu_1 + \nu_3$) and those at 3627 and 3603 cm^{-1} ($2\ \nu_2 + \nu_3$). Putting the system under vacuum reveals IR bands corresponding to (strongly) adsorbed species on the SiO_2 support in the 3000–2800 cm^{-1} region (see inset in Fig. 3). Considering the wavenumbers of these bands, they may indicate the formation of CH_x species onto the SiO_2 support. This assignment is further supported by the existence of similar bands in a CH_4/Ar system under plasma (see Fig. S23 and S24†), and the lack thereof in a CO_2/Ar system under plasma (see Fig. S20 and S21†). Interestingly, as gas phase adsorption of CH_4 onto SiO_2 occurs through weak physisorption and is fully reversible upon evacuation,[30] the adsorption behavior of CH_4 appears to be strongly modified under plasma. Indeed, it seems that new chemical bonds could be formed between CH_4 and the thermally inert SiO_2 support, likely due to the formation of CH_x radicals in plasma. Indeed, even upon exposure of the sample to temperatures up to 145 °C, these species remain adsorbed on the surface (see Fig. S26†). This already points to a first difference between plasma-catalytic and thermo-catalytic DRM, which may affect the catalytic surface reactions.

Fig. 4 shows the FTIR difference spectra at lower wavenumbers (2230–1300 cm^{-1}) recorded during DRM in plasma on the SiO_2 support. Apart from bands corresponding to gas phase CO_2 (2357 and 2336 cm^{-1}, ν_3, not shown in Fig. 4) and CO (2165 and 2120 cm^{-1}, ν_1), another, strong IR band appears at 1722 cm^{-1}. For the assignment of this band, it is important to note that (i) the band shows a similar behaviour upon increasing the temperature as the bands representing physisorbed formaldehyde (see Fig. S26 and S40†), and (ii) the band is not (or to much smaller extents) formed upon exposure of the sample to CO_2/Ar or CH_4/Ar plasma alone (see ESI,† section S5).

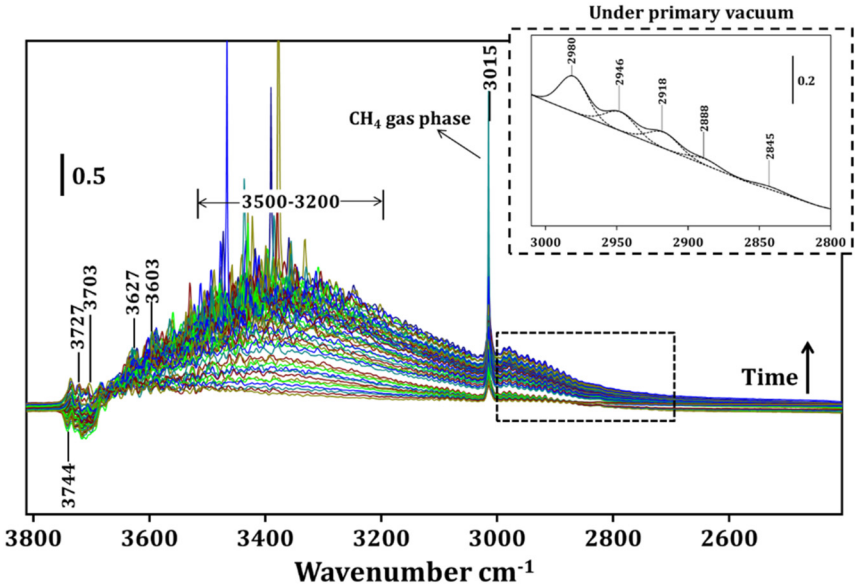

Fig. 3 FTIR difference spectra as a function of time of the SiO_2 support during DRM in plasma in the 3800–2400 cm^{-1} region with detail of the 3100–2800 cm^{-1} region. Spectra are shown with a time interval of 36 s up to steady state.

On one hand, the band could indicate the formation of chemisorbed formaldehyde species (Si–O–CH═O) on the SiO_2 support. A possible pathway towards these species on SiO_2 could be the direct adsorption of CHO, which is formed during DRM in DBD plasma, even without the presence of a catalyst, hence formed by plasma–chemical reactions.[3] However, the rather low temperature at which this band decreases, similar to the desorption temperature of formaldehyde (see (i) above), may contradict this assignment.

In this regard, assignment of the 1722 cm^{-1} band to physisorbed formic acid may be more realistic; indeed, a band at 1720 cm^{-1} has been observed for the physisorption of formic acid on SiO_2, and the simultaneous development of bands in the 1500–1400 cm^{-1} region is consistent with this assignment.[31,32] Moreover, formic acid was previously

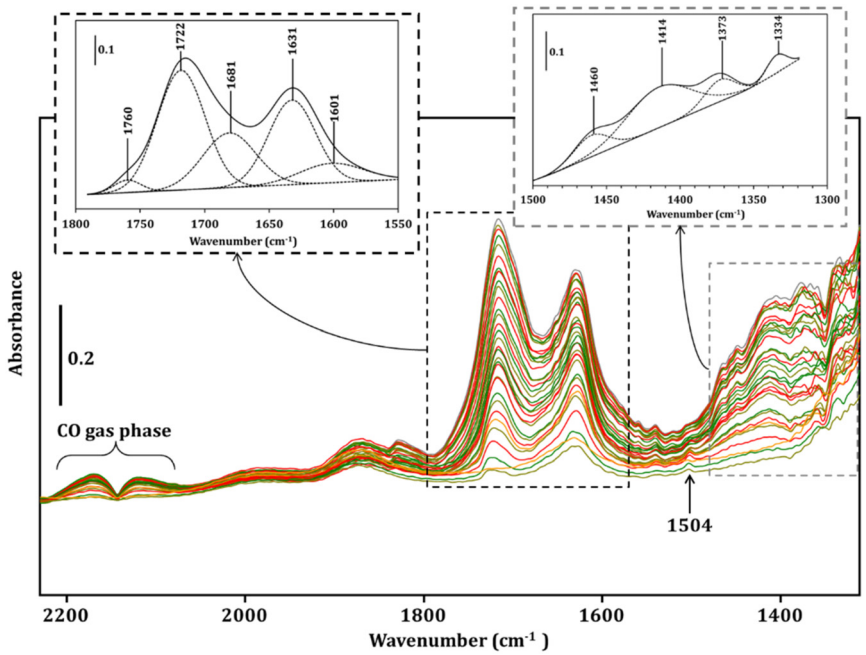

Fig. 4 FTIR difference spectra as a function of time (36 s between spectra up to steady state) of the SiO_2 support during DRM in plasma in the 2230–1300 cm^{-1} region with detail of the 1800–1550 cm^{-1} and 1500–1300 cm^{-1} regions. Spectra are shown with a time interval of 36 s up to steady state.

observed as a reaction product of plasma-catalytic DRM,[33] albeit in trace amounts, and the band at 1760 cm^{-1}, which disappears under vacuum, can be assigned to gas phase formic acid.

Furthermore, during the reaction, a band at 1631 cm^{-1} develops, which remains under vacuum (see Fig. S25†), showing the formation of adsorbed water in the plasma.

Bands at 1684 and 1381 cm^{-1}, which persist under vacuum, may evidence the presence of bicarbonate like species, whereas bands at 1596 and 1466 cm^{-1} remain under vacuum and may indicate the presence of monodentate carbonates on SiO_2, and the appearance of bands at 1668 and 1450 cm^{-1} upon switching off the plasma may evidence the formation of bidentate carbonates on SiO_2. While the latter observation may suggest that bidentate carbonates are exclusively formed in the afterglow of the plasma, alternatively, it may indicate that their destruction is discontinued upon extinguishing the plasma. It is worth noting that neither monodentate, nor bidentate carbonates are observed on SiO_2 during thermo-catalytic DRM,[34] and thus, their formation must also be attributed to plasma effects, such as Eley–Rideal reactions involving *e.g.* CO.

For an alternative representation of the evolution of the FTIR difference spectra over time, we refer the reader to waterfall plots in the ESI† (see Fig. S27).

3.2.2. 3 wt% Ru/SiO_2. A H_2/Ar plasma is first applied for *in situ* reduction of Ru on the catalyst wafer. Two minutes after plasma ignition, the formation of H_2O is observed, indicating the reduction of RuO to metallic Ru by the H_2 plasma (see Fig. S28†). Reduction is completed after 6 minutes. Afterwards, negative IR bands at 3800–3500 and ~1625 cm^{-1} are recorded, indicating that the initially adsorbed water at the catalyst surface is also desorbed.

Again, in order to disentangle the effects of the individual reactants of DRM, we performed experiments with CO_2/Ar and CH_4/Ar plasma in addition to experiments with a mixture of the reactants, the results of which are presented in Fig. S29–S35.†

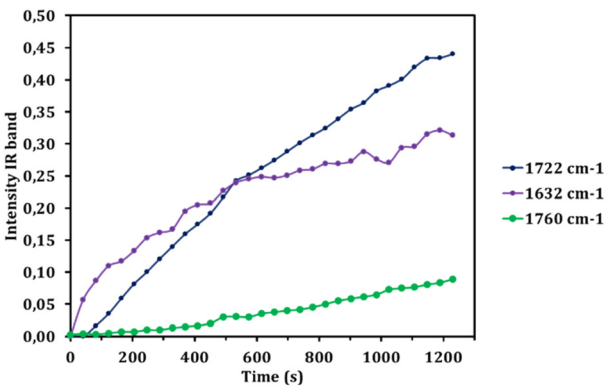

Fig. 5 Evolution of the intensity of bands observed in the FTIR spectra over time during plasma-catalytic DRM over SiO_2 at 1722 (blue), 1632 (purple) and 1760 cm^{-1} (green).

While the spectra in the 3800–2000 cm^{-1} range recorded during DRM on Ru/SiO_2 are similar to the corresponding spectra recorded on SiO_2 alone (see Fig. S36 and S37†), the 2000–1300 cm^{-1} region shows a remarkable difference (see Fig. 6 and S36†). More specifically, the band at 1722 cm^{-1} that was previously observed on the SiO_2 support and assigned to adsorbed formic acid exhibits a much lower intensity, and the amount of adsorbed water on the catalyst surface is much smaller as well, as evidenced by the vast decrease in intensity of the 1631 cm^{-1} band on Ru/SiO_2 compared to SiO_2. Indeed, on Ru/SiO_2, both bands exhibit about half of the intensity they show on SiO_2.

Interestingly, when looking at the development of both bands over time on SiO_2 alone (see Fig. 5), water is immediately formed on the surface upon switching the plasma on, whereas formic acid is formed with some delay. This could indicate that the water on the catalyst surface serves as a source of OH groups for the formation of formic acid from, for example, CHO, which is a known reactive species in DRM in plasma.[3] We observe a similar delay on Ru/SiO_2, although the intensity of the bands is much lower. Note that the 1760 cm^{-1} band, illustrative of gas phase formic acid, initially shows a low intensity, which increases as the reaction progresses, potentially showing desorption of physisorbed formic acid from the SiO_2 surface.

We hypothesize that the difference in adsorbed water between both samples can be attributed to the surface temperature. Indeed, the presence of water vapour in the plasma with Ru/SiO_2 catalyst is clearly visible in Fig. 6, whereas the same bands are not observed in the plasma with SiO_2. This is a good indication that while on SiO_2, the plasma remains at a low temperature, the temperature of the plasma on Ru/SiO_2 is elevated above 100 °C, which is indeed confirmed in section 3.2.3. At these elevated temperatures, the amount of surface adsorbed water is low, so that the formation of formic acid is limited. It should be mentioned that temperature-induced desorption of formic acid cannot be excluded at these temperatures (see Fig. S26†), which would contribute to a lower intensity of the 1722 cm^{-1} band.

While it is not yet clear to what extent formic acid adsorbed on SiO_2 exactly contributes to the plasma-catalytic reaction, its formation is remarkable, and has, to the best of our knowledge, not yet been considered in plasma-catalytic DRM.

Clearly, this type of interaction between the plasma species and the catalyst differs from the classical interpretation of catalysis in a thermal system. Indeed, in the latter, catalytic activity is determined by the available pathways in which reactants can be converted to reaction products on the catalytic surface, with the Langmuir–Hinshelwood mechanism being dominant. While these surface reactions can also play a role in plasma catalysis, clearly, the role of a plasma catalyst goes beyond that. In the present work, we have illustrated that the plasma-induced heating of the catalyst surface is dependent on the catalyst

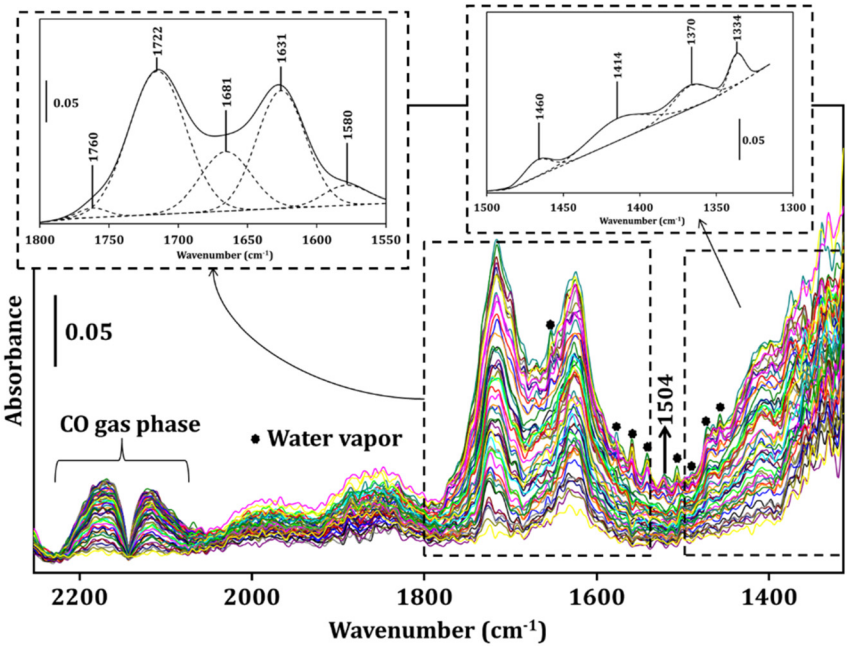

Fig. 6 FTIR difference spectra as a function of time (up to steady state) of the 3 wt% Ru/SiO_2 catalyst during DRM in plasma in the 2000–1300 cm^{-1} region with detail of the 1250–1950 cm^{-1} region. Spectra are shown with a time interval of 36 s up to steady state.

material, which in its turn affects the plasma-induced adsorption on the catalyst surface.

3.2.3. Estimation of catalyst temperature under DBD plasma. In order to better understand whether the formation of surface species is due to plasma-induced surface heating or other plasma effects, such as plasma-generated radicals, we need to know the catalyst surface temperature, determined with the method explained in section 2.2.3 above. Fig. 7 shows the evolution of the wavenumber of the $BaSO_4$ band $\bar{\nu}_{max}$ (see eqn (1) in section 2.2.3), used to probe the temperature of the pure $BaSO_4$ sample, along with the corresponding temperature, as a function of time in a H_2/Ar DBD plasma. We select this as a simple system with limited chemistry to first illustrate our novel technique in a comprehensible way. While it clearly shows that switching on the plasma leads to a roughly continuous temperature increase up to ~90 °C, with a stabilization after ~15–20 min, there is no clear relation between applied voltage and observed temperature. Moreover, the applied voltage does not greatly influence the heating rate of the sample, and upon plasma extinction, the sample temperature again drops to its initial temperature at rates similar to those observed for the temperature increase.

The position of the maximum of the $BaSO_4$ band used to probe the temperature of the $Ru/SiO_2/BaSO_4$ system as a function of time in a CO_2/CH_4/Ar plasma, along with the

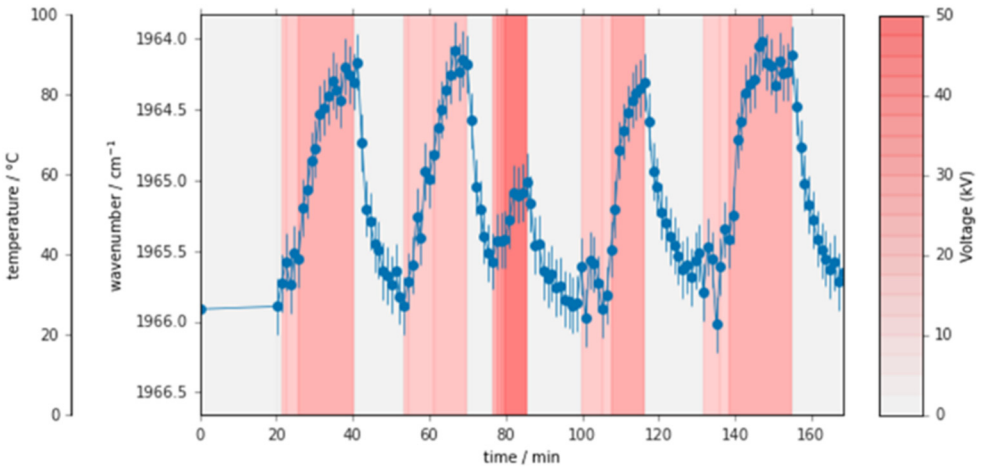

Fig. 7 Wavenumber of the $BaSO_4$ band used to probe the $BaSO_4$ temperature in a H_2/Ar DBD plasma as a function of time. The intensity of the background color is indicative of the applied voltage, going from grey (0 kV, plasma off) to dark red (50 kV).

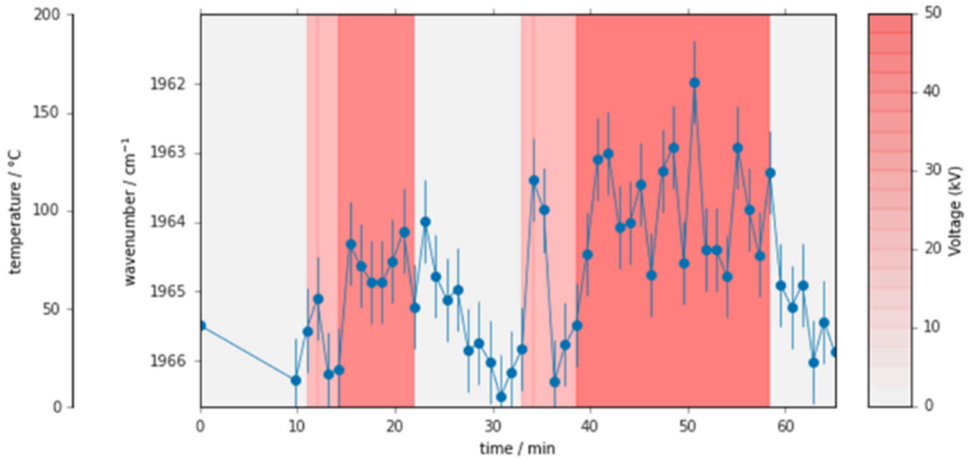

Fig. 8 Wavenumber of the $BaSO_4$ band used to probe the $Ru/SiO_2/BaSO_4$ temperature in a $CO_2/CH_4/Ar$ DBD plasma as a function of time. The intensity of the background color is indicative of the applied voltage, going from grey (0 kV, plasma off) to dark red (50 kV).

corresponding temperature, is shown in Fig. 8. In this case, while the data are noisier than for pure $BaSO_4$ due to dilution, the trends are still clear and we observed a temperature increase in the range of 70–120 °C, with peaks up to 150 °C. Hence, the maximum temperature of the Ru/SiO_2 wafer during the plasma-catalytic DRM can be estimated to be lower than 150 °C. We also performed experiments in a thermal *in situ operando* IR "sandwich cell", as described in section 2.2.4 and in section S6 of the ESI† (see Fig. S38†). Our spectra (see Fig. S39†) reveal that this temperature increase is insufficient for the formation of surface species on the catalyst sample, as well as for the conversion of CO_2 and CH_4 (*i.e.* our samples exhibit no activity at this temperature), which was not observed in our thermal *in situ operando* cell, even at 450 °C. Hence, the formation of the species at the catalyst surface and the conversion of CO_2 and CH_4 must be attributed to effects other than plasma-induced surface heating, such as the adsorption of plasma-generated radicals or molecules, or the occurrence of Eley–Rideal reactions.

Note that the field of plasma catalysis is greatly hindered by a lack of understanding of the actual role of plasma-induced surface heating in possible synergism,[37] and therefore, these observations provide a valuable contribution towards a better understanding of plasma-catalytic synergism by the decoupling of thermal and plasma effects.

3.3. Packed bed DBD experiments

Table 1 shows the CO_2 and CH_4 conversion, as well as the product yields and selectivities, obtained in the packed bed DBD reactor, for both the SiO_2 support and the 3 wt% Ru/SiO_2 catalyst. Besides H_2 and CO, which are the major products of DRM (*i.e.* syngas), C_2H_4 is produced in non-negligible amounts. Note that the yield and selectivity are H-based for H_2, and C-based for CO and C_2H_4.

The CO_2 and CH_4 conversions are lower for the Ru/SiO_2 catalyst than for the bare SiO_2 support, as well as the selectivity towards syngas (both to H_2 and CO). Moreover, the C_2H_4 selectivity is significantly higher on Ru/SiO_2, *i.e.*, 3.1% *vs.* 1.2% for the bare SiO_2 support. We hypothesize that these results can indeed (at least partly) be understood with the findings in our *in situ* cell. Indeed, the conversions of CO_2 and CH_4 are to a great extent determined by backreactions of plasma species, *i.e.* reactions in which the initial reactants (CO_2 and CH_4) are formed again. These reactions involve CHO and OH,[3] the concentrations of which are reduced by

Table 1 CO_2 and CH_4 conversion, and H_2, CO and C_2H_4 yield and selectivity obtained for the plasma-catalytic DRM over SiO_2 and 3 wt% Ru/SiO_2 in a packed bed DBD reactor

		SiO_2 extrudates	3 wt% Ru/SiO_2 extrudates
CO_2 conversion (%)		17 ± 2	10 ± 2
CH_4 conversion (%)		25.4 ± 0.5	19 ± 2
H_2	Yield (%)	22.3 ± 0.4	11.6 ± 0.9
	Selectivity (%)	87.9 ± 0.1	61 ± 4
CO	Yield (%)	17.1 ± 0.6	7.2 ± 0.9
	Selectivity (%)	81 ± 3	50 ± 6
C_2H_4 (ethylene)	Yield (%)	0.46	0.65
	Selectivity (%)	1.2	3.1

The H_2 yield and selectivity are H-based, while the CO and C_2H_4 yield and selectivity are C-based (see formulas in ESI,† section S2). Error bars for C_2H_4 yield and selectivity are not available, since C_2H_4 production was only monitored with FTIR during one experiment.

the formation of formic acid on the SiO_2 surface, which could reduce the contribution of these backreactions, and thus increase the CO_2 and CH_4 conversion. Note that during plasma operation, condensate is visibly formed at the reactor outlet, so that an accurate detection of liquid reaction products like CH_3OH or formic acid during steady-state plasma operation was not possible.

4. Conclusions

In this work, we present an *in situ* study (*i.e.* inside the plasma and during operation) of the infrared-active species formed on the surface of (Ru-loaded) silica during plasma-catalytic DRM using a novel *in situ* transmission IR DBD cell. Moreover, to link the observations of the *in situ* experiments to catalytic activity, we also tested the catalysts in a packed bed DBD reactor, and we measured the CO_2 and CH_4 conversion and product yields and selectivities. We found that in the plasma-catalytic DRM on SiO_2, adsorbed water is immediately formed, while adsorbed formic acid is formed with a delay, possibly indicating that water provides OH for the formation of formic acid. We hypothesize that, as Ru/SiO_2 is subject to greater plasma-induced surface heating, the amount of adsorbed water is lower, leading to less formation of formic acid on this catalyst.

In addition, we present a novel technique to estimate the temperature of the catalyst inside our plasma-catalytic system *in situ*, and found a maximum catalyst temperature increase in the range of 70–120 °C, with peaks up to 150 °C for Ru/SiO_2. This temperature increase is insufficient for the formation of surface-adsorbed species on the catalyst, as revealed by our experiments in a thermal *in situ operando* IR "sandwich" cell. Hence, the formation of these species cannot be attributed to plasma-induced heating, but must be due to other plasma effects, such as the adsorption of plasma-generated radicals, molecules or the occurrence of Eley–Rideal reactions. This novel technique thus allows to decouple thermal and plasma effects, and therefore, it contributes greatly towards a better understanding of plasma-catalytic synergism.

In general, our study provides valuable insights in the occurrence of surface-adsorbed species that may play a role in plasma-catalytic DRM. Nevertheless, more work is needed to obtain a comprehensive picture of the entire mechanism. A better understanding of the surface reactions could be obtained by for example Steady-State Isotopic Transient Kinetic Analysis (SSITKA) and step-scan FTIR analysis. Additionally, combining the obtained experimental results with plasma–chemical and microkinetic surface chemistry models, in which the fundamental reaction steps on the catalyst surface and in the plasma are modelled, could lead to a better understanding of the observed experimental results, and thus provide an overall picture of the underlying interactions between the plasma and a catalyst in plasma-catalytic DRM.

Conflicts of interest

There are no conflicts to declare.

Acknowledgements

This research was supported by the European Research Council (ERC) under the European Union's Horizon 2020 Research and Innovation programme (grant agreement No. 810182 – SCOPE ERC Synergy project) and the European Union's Horizon 2020 Research and Innovation programme under the Marie Sklodowska-Curie grant agreement No. 813393 (PIONEER).

References

1 G. A. Mills, *Fuel*, 1994, **73**, 1243–1279.
2 A. Bogaerts, E. Neyts, R. Gijbels and J. van der Mullen, *Spectrochim. Acta, Part B*, 2002, **57**, 609–658.
3 R. Snoeckx, R. Aerts, X. Tu and A. Bogaerts, *J. Phys. Chem. C*, 2013, **117**, 4957–4970.
4 A. Bogaerts, T. Kozak, K. van Laer and R. Snoeckx, *Faraday Discuss.*, 2015, **183**, 217–232.
5 J. C. Whitehead, *J. Phys. D: Appl. Phys.*, 2016, **49**, 243001.
6 E. Neyts, K. K. Ostrikov, M. K. Sunkara and A. Bogaerts, *Chem. Rev.*, 2015, **115**, 13408–13446.
7 A.-J. Zhang, A.-M. Zhu, J. Guo, Y. Xu and C. Shi, *Chem. Eng. J.*, 2010, **156**, 601–606.
8 L. B. F. Juurlink, D. R. Killelea and A. L. Utz, *Prog. Surf. Sci.*, 2009, **84**, 69–134.
9 L. Wang, Y. Zhao, C. Liu, W. Gong and H. Guo, *Chem. Commun.*, 2013, **49**, 3787–3789.
10 S. Xu, S. Chansai, S. Xu, C. E. Stere, Y. Jiao, S. Yang, C. Hardacre and X. Fan, *ACS Catal.*, 2020, **10**, 12828–12840.
11 U. Kogelschatz, B. Eliasson and W. Egli, *J. Phys. IV*, 1997, **7**, 47–66.
12 R. Snoeckx and A. Bogaerts, *Chem. Soc. Rev.*, 2017, **46**, 5805–5863.
13 R. J. Baxter and P. Hu, *J. Chem. Phys.*, 2002, **116**, 4379–4381.
14 Y. Engelmann, K. van't Veer, Y. Gorbanev, E. C. Neyts, W. F. Schneider and A. Bogaerts, *ACS Sustainable Chem. Eng.*, 2021, **9**, 13151–13163.
15 J. Lee, D. C. Sorescu and X. Deng, *J. Am. Chem. Soc.*, 2011, **133**, 10066–10069.
16 P. Mehta, P. Barboun, F. A. Herrera, J. Kim, P. Rumbach, D. B. Go, J. C. Hicks and W. F. Schneider, *Nat. Catal.*, 2018, **1**, 269–275.
17 R. Michiels, Y. Engelmann and A. Bogaerts, *J. Phys. Chem. C*, 2020, **124**, 25859–25872.
18 Y. Engelmann, P. Mehta, E. C. Neyts, W. F. Schneider and A. Bogaerts, *ACS Sustainable Chem. Eng.*, 2020, **8**, 6043–6054.
19 B. Loenders, Y. Engelmann and A. Bogaerts, *J. Phys. Chem. C*, 2021, **125**, 2966–2983.
20 A. Rodrigues, J.-M. Tatibouët and E. Fourré, *Plasma Chem. Plasma Process.*, 2016, **36**, 901–915.
21 C. Stere, S. Chansai, R. Gholami, K. Wangkawong, A. Singhania, A. Goguet, B. Inceesungvorn and C. Hardacre, *Catal. Sci. Technol.*, 2020, **10**, 1458–1466.

22 R. Vakili, R. Gholami, C. E. Stere, S. Chansai, H. Chen, S. M. Holmes, Y. Jiao, C. Hardacre and X. Fan, *Appl. Catal., B*, 2020, **260**, 118195.
23 A. Parastaev, N. Kosinov and E. J. M. Hensen, *J. Phys. D: Appl. Phys.*, 2021, **54**, 264004.
24 F. Thibault-Starzyk and J. Saussey, Infrared Spectroscopy: Classical Methods, in *In-situ Spectroscopy of Catalysts*, American Scientific Publishers, San Diego, 2004, pp. 15–31.
25 F. Azzolina-Jury and F. Thibault-Starzyk, *Top. Catal.*, 2017, **60**, 1709–1721.
26 H. Li, F. Rivallan, A. Thibault-Starzyk, A. Travert and F. C. Meunier, *Phys. Chem. Chem. Phys.*, 2013, **15**, 7321–7327.
27 Y. Sun, J. Li, P. Chen, B. Wang, J. Wu, M. Fu, L. Chen and D. Ye, *Appl. Catal., A*, 2020, **591**, 117407.
28 M. Safariamin, L. H. Tidahy, E. Abi-Aad, S. Siffert and A. Aboukaïs, *C. R. Chim.*, 2009, **12**, 748–753.
29 E. K. Gibson, C. E. Stere, B. Curran-McAteer, W. Jones, G. Cibin, D. Gianolio, A. Goguet, P. P. Wells, C. R. A. Catlow, P. Collier, P. Hinde and C. Hardacre, *Angew. Chem., Int. Ed.*, 2017, **56**, 9351–9355.
30 H. Hattori, P. Arudra, A. Abdalla, A. M. Aitani and S. S. Al-Khattaf, *Catal. Lett.*, 2019, **150**, 771–780.
31 G. J. Millar, C. H. Rochester and K. C. Waugh, *J. Chem. Soc., Faraday Trans.*, 1991, **87**, 1491–1496.
32 F. Solymosi, A. Erdöhelyi and T. Bánsági, *J. Chem. Soc., Faraday Trans. 1*, 1981, **77**, 2645–2657.
33 M. Magureanu and C. Bradu, *Catalysts*, 2021, **11**, 1439.
34 P. Ferreira-Aparicio, I. Rodríguez-Ramos, J. A. Anderson and A. Guerrero-Ruiz, *Appl. Catal., A*, 2000, **202**, 183–196.
35 J. Manam and S. Das, *Radiat. Eff. Defects Solids*, 2008, **163**, 955–965.
36 K. Nakamoto, *Infrared and Raman Spectra of Inorganic and Coordination Compounds: Part A: Theory and Applications in Inorganic Chemistry*, John Wiley & sons, 2008.
37 E. C. Lovell, J. Scott, N. M. Bedford, T. H. Tan, P. J. Cullen, K. K. Ostrikov and R. Amal, *ACS Energy Lett.*, 2022, **7**, 300–309.
38 A. Travert and C. Fernandez, *SpectroChemPy (Version 0.2.17), Zenodo*, 2021, DOI: **10.5281/zenodo.3823841**.
39 A. Travert and C. Fernandez, *SpectroChemPy (Version 0.2.17)*, 2021, (accessed 2021-01-28), **https://www.spectrochempy.fr**.
40 R. J. Clarke and J. C. Hicks, *ACS Eng. Au*, 2022, DOI: **10.1021/acsengineeringau.2c00026**.
41 M. Rivallan, E. Fourré, S. Aiello, J. M. Tatibouët and F. Thibault-Starzyk, *Plasma Processes Polym.*, 2012, **9**, 850–854.